Spatiotemporal properties of intrinsic sea level variability along the Southeast United States coastline

Carmine Donatelli[1], Christopher M. Little[1], Rui M. Ponte[1], Stephen G. Yeager[2]

[1]Atmospheric and Environmental Research, Lexington (MA), USA
5   [2]National Center for Atmospheric Research, Boulder (CO), USA

Correspondence to: Carmine Donatelli (cdonatelli@aer.com)

Abstract. The influence of intrinsic ocean variability on coastal sea level remains largely unexplored but is of potential importance for emerging forecasting efforts. As in weather forecasts, intrinsic variability will amplify uncertainty in initial conditions. However, variability originating from intrinsic processes may be predictable in a forecast system with sufficient
10   resolution and accurate initialization. Here, we examine the spatiotemporal properties of intrinsic sea level variability along the Southeast United States coast using a suite of global ocean/sea-ice simulations at 0.1° horizontal resolution. In model simulations, intrinsic variability is a dominant component of the monthly de-seasonalized and detrended sea level variability in deep waters, but it is damped along continental shelves, where it comprises ~10-30% of the sea level standard deviation. Our analyses demonstrate that US East Coast and Gulf of Mexico shelves exhibit a common intrinsic mode, with maximal
15   amplitude in the South Atlantic Bight and almost no expression north of Cape Hatteras. This intrinsic coastal mode is coherent with sea level along the Gulf Stream axis after detachment from Cape Hatteras. Intrinsic sea level variability in the detached Gulf Stream leads the coastal mode by 2-3 months, suggesting that intrinsic coastal sea level variability may exhibit predictability.

1 Introduction

Coastal ecosystems, communities, and economies are highly susceptible to sea level variability over a wide range of time scales (e.g., Rashid et al., 2021; NOAA, 2022). Accurate sea level predictions are needed for mitigation and adaptation
25   purposes and for effectively managing risks associated with sea level variability. Such predictions will benefit from: 1) improved understanding of relevant drivers of regional coastal sea level variability, and 2) assessment of the representation of monthly to interannual coastal sea level variability in dynamic models utilized for operational ocean forecasting. Various physical processes operating at different spatial and temporal scales influence sea level variability (e.g., Gerkema & Duran-Matute, 2017; Little et al., 2019; Camargo et al., 2024). These processes can be partitioned into a deterministic

30   component that occurs in response to an applied forcing ("atmospherically-forced component"), and a non-deterministic ("intrinsic") component, which is not directly driven by atmospheric variability but is instead generated by the ocean itself, for instance, through small-scale (i.e., mesoscale and smaller) turbulent processes (e.g., Penduff et al., 2011). Such small-scale processes become particularly important in eddy-active regions of the ocean and cause the ocean's evolution to be non-deterministic at both small and large (regional to basin) scales under prescribed forcing conditions (Sérazin et al., 2015; Qiu

35   et al., 2015; Forget & Ponte, 2015; Close et al., 2020).

Sea level variability originating from intrinsic processes might be a significant source of uncertainty in forecasts and can only be represented by adopting ocean models of sufficient horizontal resolution (e.g., Penduff et al., 2010; 2011; Sérazin et al., 2018; Chassignet et al., 2020). However, generally, the horizontal resolution of ocean models used for coastal sea level forecasts is on the order of 1° (~100 km), which is insufficient to capture the effect of oceanic intrinsic variability on coastal

40   sea level (e.g., Long et al., 2021).

Even in simulations capable of representing intrinsic processes, separation of forced and intrinsic variability is not trivial. Two strategies have been used to isolate the contribution of intrinsic variability in eddy-permitting ocean model simulations. The first strategy compares model output from a realistic atmospherically forced model with one only subjected to climatological forcing (e.g., Stewart et al., 2020) (i.e., repeat-year forcing simulations). The second approach employs

45   ensemble members with perturbed initial conditions, which permit the estimation of the forced (ensemble mean) and intrinsic components (i.e., difference between time series of a specific member and the ensemble mean) (e.g., Penduff et al., 2014; Bessières et al., 2017; Donatelli et al., 2025).

This paper focuses on characterizing the spatiotemporal properties of intrinsic sea level variability along the Southeast Coast of the United States (including the Gulf of Mexico), where societal vulnerability to sea level variability is high and

50   increasing (e.g., Thatcher et al., 2013). The majority of the studies in this area focus on atmospherically-forced variability (e.g., Frederikse et al., 2017; Calafat et al., 2018; Piecuch et al., 2018; Wang et al., 2024) and less is known about the influence of oceanic intrinsic processes on coastal sea level.

The Southeast Coast of the United States (from now on, SEUS) has a strong intrinsic component at sub-annual to interannual timescales (e.g., Close et al., 2020; Little et al. 2024). However, previous studies do not elucidate: (i) the SEUS along-coast

55   spatial structure, and (ii) how coastal variability relates to offshore variability over space and time. To explore these questions, it is essential to use simulations that: 1) represent the SEUS shelf topography with sufficient grid points even in regions where the shelf narrows, and 2) adequately resolve offshore intrinsic variability (e.g., Halberg et al., 2013).

Here, to study the spatial structure (and magnitude) of intrinsic sea level variability along the SEUS coastline and its spatiotemporal relationship with offshore variability, we utilize monthly sea surface height (SSH) fields from high-resolution

60   (HR) forced ocean/sea-ice (FOSI) and repeat-year-forcing (RYF) (Stewart et al., 2020) simulations performed using the Community Earth System Model at 0.1° horizontal resolution (Chang et al., 2020; Yeager et al., 2023; Little et al., 2024). We utilized the HR FOSI simulation to evaluate whether the model faithfully represents observations, and the HR RYF simulation to cleanly estimate intrinsic sea level variability. The paper is organized as follows. The model setup,

observational datasets, and data processing are described in the Appendix. In Section 2, we show the results, and in Section
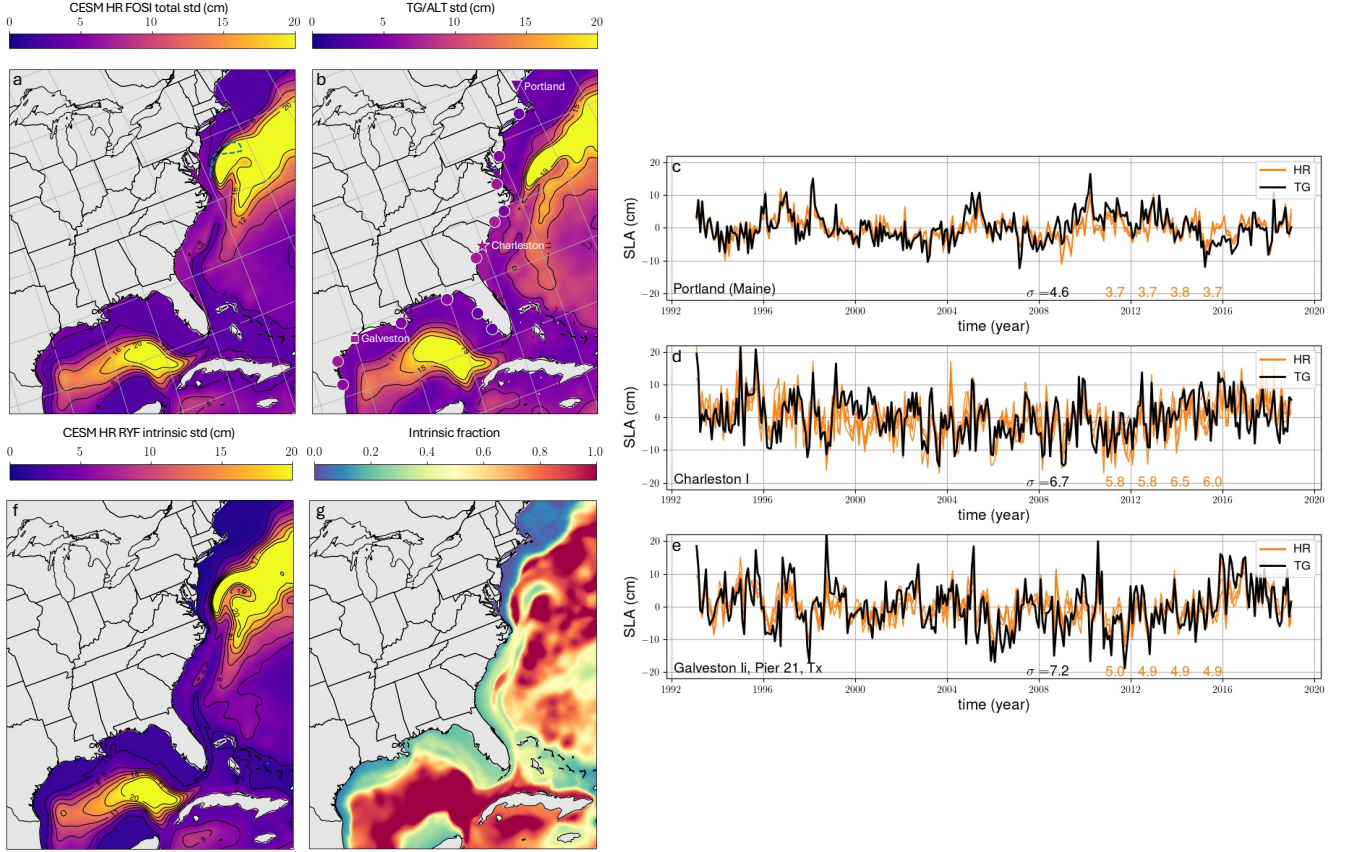3, we present the discussion and conclusions.

Figure 1: Total sea level standard deviation (cm) from (a) the HR FOSI simulation (the blue dashed line indicates the offshore region in Fig. 3a) and (b) gridded altimeter product over the period 1993-2015. (c, d, e) Comparison between detrended and de-seasonalized time series from tide gauges (TGs) and HR FOSI ensemble simulation in three representative locations. We reported the standard deviation (cm) for TGs (black) and each FOSI cycle. The location of each TG is shown in Fig. 1b. (f) Intrinsic standard deviation (cm) estimated using the HR RYF simulation. (g) Intrinsic fraction (i.e., intrinsic standard deviation estimated from the HR RYF simulation divided by total standard deviation computed using the HR FOSI simulation).

2 Results

2.1 Total and intrinsic sea level variability

We first compare the total (i.e., forced plus intrinsic) sea level standard deviation from the HR FOSI simulation and observations over the 1993-2018 period (Fig. 1). Total sea level standard deviation (mean across the FOSI members; Fig. 1a) is larger in deep waters and decreases over the continental shelf. Over the same temporal window, a gridded altimeter product (Fig. 1b) shows a similar spatial structure, with the model generally underestimating the observed monthly total sea level standard deviation over the shelf by 10-20%. A similar result was obtained when we compared coastal grid points with

3

the detrended and de-seasonalized sea level recorded by tide gauges (TGs). At three representative locations along the US coastline (Figs. 1c, d, e), discrepancies between model and TG observations were more significant in Galveston (see standard deviations in Figs. 1c, d, e). In contrast, Charleston exhibited the largest inter-cycle differences. Our results show that, overall, sea level hindcasts compare favorably to TG observations over the 1993-2018 period (see Table 1).

Tide gauge	R^2	RMSE (cm)
Portland (Maine)	0.81, 0.80, 0.78, 0.8	2.70, 2.73, 2.88, 2.79
New Port	0.80, 0.78, 0.78, 0.79	2.52, 2.63, 2.65, 2.59
Cape May	0.86, 0.86, 0.85, 0.86	2.80, 2.85, 2.90, 2.85
Sewells Point, Hampton Roads	0.85, 0.85, 0.85, 0.85	3.51, 3.57, 3.53, 3.54
Beaufort (North Carolina)	0.70, 0.69, 0.73, 0.71	4.01, 4.11, 3.93, 3.99
Wilmington	0.49, 0.51, 0.54, 0.52	6.77, 6.72, 6.62, 6.66
Charleston	0.66, 0.71, 0.73, 0.66	5.19, 4.85, 4.79, 5.22
Fort Pulaski	0.64, 0.68, 0.71, 0.63	5.62, 5.27, 5.32, 5.75
Naples	0.41, 0.43, 0.51, 0.43	4.10, 3.92, 3.73, 3.94
St. Petersburg	0.48, 0.46, 0.53, 0.44	3.85, 3.79, 3.60, 3.93
Apalachicola	0.57, 0.54, 0.58, 0.52	4.80, 4.90, 4.73, 5.02
Grand Isle	0.67, 0.67, 0.72, 0.66	3.99, 3.95, 3.68, 4.00
Galveston	0.76, 0.78, 0.81, 0.75	4.76, 4.59, 4.37, 4.80
Rockport	0.73, 0.75, 0.77, 0.73	4.42, 4.37, 3.98, 4.65
Port Isabel (Texas)	0.7, 0.72, 0.75, 0.71	4.21, 4.05, 3.82, 4.15

Table 1. Comparison between HR FOSI simulation and TG observations. For each ensemble member, we reported coefficient of determination (R^2) and root mean square error (RMSE).

We next quantify intrinsic variability using detrended and de-seasonalized monthly outputs from the HR RYF simulation (Fig. 1f). The intrinsic standard deviation shows substantial spatial variations; specifically, it is damped on the continental shelf relative to offshore. By computing the intrinsic fraction (i.e., ratio between the intrinsic standard deviation from the HR RYF simulation and the total cycle-mean sea level standard deviation from the HR FOSI simulation), we found that the intrinsic standard deviation represents 10-30% of the total sea level standard deviation on the continental shelf south of Cape Hatteras and up to 100% of the total standard deviation in deep waters (Fig. 1g; note that these results pertain to a region dominated by a western boundary current). Offshore intrinsic variability is maximized in the interior of the Gulf of Mexico and in proximity to the Gulf Stream (GS). Along the GS path, we found a minimum in the offshore intrinsic fraction (Fig. 1g), which coincides with a region of low intrinsic standard deviation (Fig. 1f). The core of the GS is characterized by weaker zonal SSH gradients with respect to its margins (see SSH contours in Fig. 3). These spatial variations in SSH gradients may be responsible for the patterns observed in offshore intrinsic variability near the GS.

2.2 Intrinsic sea level variability along the SEUS coast

100   We utilized detrended and de-seasonalized monthly SSHs extracted at 170 coastal grid points (pseudo-TGs) from the HR RYF simulation to analyze the spatial structure of intrinsic sea level variability along the SEUS coast. Consistent with Figs. 1f, g, coastal grid points exhibit minimal variability north of Cape Hatters (see pseudo-TGs between locations 100 and 170 in Fig. 2a).

We used EOF analysis to identify the modes that explain the largest fraction of the variability along the SEUS coastline. The
105   EOF decomposition revealed that the first two modes explain most of the variability in the dataset. Specifically, the first mode explains 73% of the variability, while the second mode contributes 12% (Figs. 2b, c). The eigenvector associated with the dominant mode showed the same sign in all the pseudo-TGs (as indicated by the color of the circles in Fig. 2b), revealing a "common mode" linking the East Coast and the Gulf of Mexico. In contrast, the second eigenvector suggests that the pseudo-TGs along the US East Coast behave opposite to those in the Gulf of Mexico (Fig. 2c). The variability explained by
110   each mode presents significant spatial variations (see the size of the circles in Figs. 2b, c), particularly between pseudo-TGs south of Cape Hatteras (larger) and those north of Cape Hatteras (smaller standard deviation). Both modes show enhanced variability between Cape Hatteras and Jacksonville.

The temporal evolution of the first two eigenvectors is represented by the PCs associated with each mode (Fig. 2d). The PCs exhibit fluctuations at sub-annual to interannual time scales, including multi-year sea level trends (for example PC1, over a
115   5-year period beginning around month 90) (Penduff et al., 2019). The remainder of the paper considers only the first mode (PC1) given its dominant role in explaining SEUS intrinsic coastal variability.
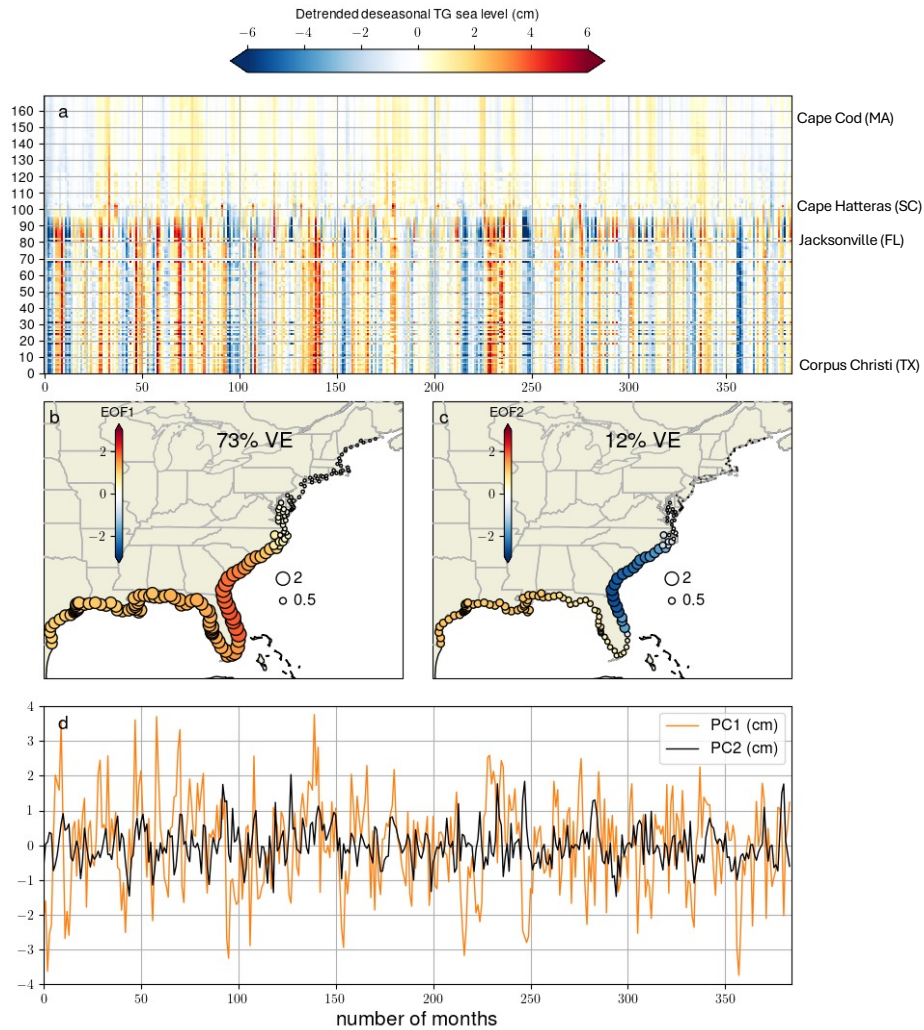
Figure 2: (a) Monthly time series from the HR RYF simulation extracted at 170 pseudo-TGs along the SEUS coastline. These time series are 32 years long. (b) First and (c) second mode obtained from EOF analysis. The color of the circles indicates the eigenvectors' value in each pseudo-TG, while the circles' radius is related to the magnitude. (d) Principal components (PCs, cm) associated with modes 1 and 2.

2.3 Relationship between along-coast and offshore intrinsic sea level variability

We utilized detrended and de-seasonalized SSH fields obtained from the HR RYF simulation to identify spatial pathways connecting offshore and coastal intrinsic sea level variability. With no lag, PC1 correlates with (i) SSHs over the entire continental shelf south of Cape Hatteras, and (ii) SSHs within an off-shelf region located in proximity to the GS axis after detachment from Cape Hatteras (Fig. 3a).

To assess evidence for propagating oceanic signals, lag correlations at different lags were applied, with a positive lag indicating that offshore sea level leads PC1. We highlight correlated off-shelf regions (blue contours in Figs. 3b, c, d) using a threshold of 0.3 (note that coherence analysis performed in the following paragraph is not sensitive to the precise threshold

6

employed to identify the detachment region). Interestingly, lag correlations reveal that the off-shelf region (i) moves

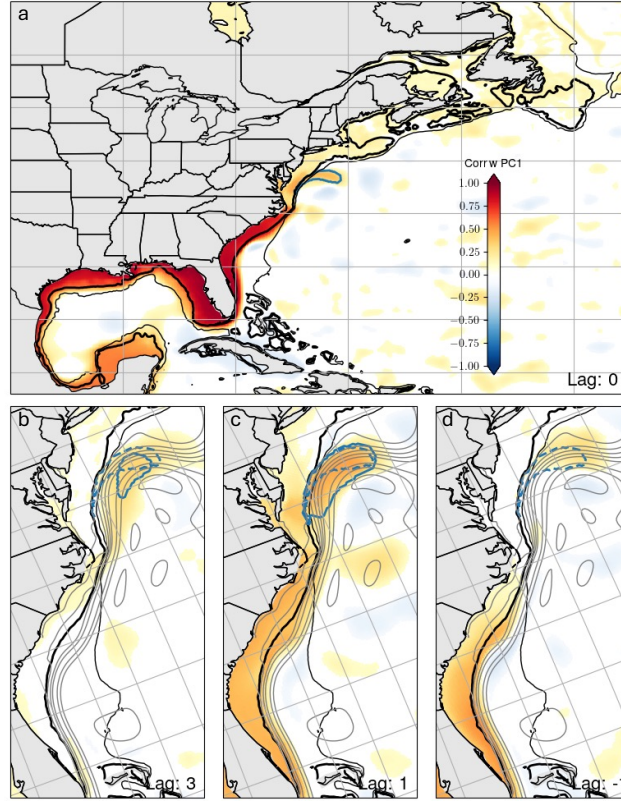130   westward and varies in size with decreasing time lag, and (ii) leads the along-coast intrinsic mode.

Figure 3: Lag correlations between the PC1 and SSH field: (a) no lag, (b) lag of 3 months, (c) lag of 1 month, and (d) lag of -1 month. A positive lag means that SSH field leads the PC1. The solid blue line in 3a shows the off-shelf region when no lag is applied to the PC1. The solid lines in 3b, c represent the off-shelf region when lags of (b) 3 months and (c) 1 month are applied to the PC1. The dashed lines in
135   3b, c, and d show the off-shelf region when no lag is applied to the PC1 (i.e., the dashed lines are the same as the solid line in 3a). The statistical significance of the lag correlations was evaluated using a *p-value* of 0.05. The thicker black lines indicate a water depth of 100 meters, while the lighter black line indicates a water depth of 1000 meters. The grey lines are time-mean SSH contours at 10-cm intervals.

We employed a spectral approach to further characterize the relationship between the PC1 and the detrended and de-

seasonalized SSHs over the off-shelf region (i.e., solid blue line in Fig. 3a). The two-time series show high coherence values

140   (coherence amplitude greater than 0.5, Fig. 4a) for frequencies smaller than 0.9 year^{-1}. In this frequency band, the coherence

phase lag (positive phase lag denotes off-shelf region leads the PC1; shown only for frequency bands where coherence is

statistically significant) ranges between 20 and 40 degrees (i.e., off-shelf region leads PC1 by 2-3 months). To help visualize

these results, we applied a 13-month low-pass filter to the two-time series (Fig. 4b). Consistent with Fig. 4a, the two filtered

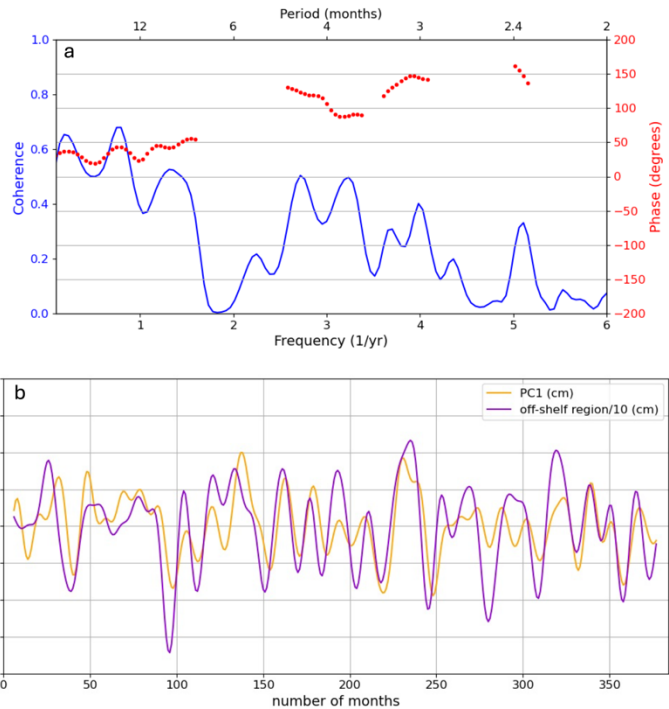signals show that the off-shelf region leads the along-coast intrinsic mode.

Figure 4: (a) Coherence analysis between the PC1 and average SSH signal within the off-shelf region. Note phase lag is only shown for statistically significant coherence (a positive phase means that the off-shelf region leads the PC1). (b) PC1 (cm) and average SSH signal (cm) within the off-shelf region to which we applied a 13-month low-pass filter. The average SSH signal within the off-shelf region is divided by 10.

3 Discussion and Conclusions

Using a 50-member ocean ensemble hindcast at 0.25° horizontal resolution, Close et al. (2020) showed that sea level variability is almost entirely driven by intrinsic processes in energetic regions of the ocean, such as the GS. Building on this study, we utilized a set of numerical experiments at higher spatial resolution to explore the linkage between offshore and coastal sea level variability along the SEUS coastline.

Our analyses revealed that, at monthly to interannual timescales south of Cape Hatteras, intrinsic processes meaningfully contribute to sea level variability, reaching up to 30% of the total monthly sea level standard deviation on the continental shelf. A common intrinsic sea level mode, largest between Charleston and the Florida Straits, but coherent around the Gulf of Mexico, is correlated with sea level variability in the detached GS through a large-scale pathway connecting deep and shelf waters. The absence of intrinsic variability to the north of Cape Hatteras is consistent with the limited ability of eddies to influence sea level where the shelf is wide (e.g., Gangopadhyay et al., 2020), and the equatorward propagation of coastal sea level anomalies originating near the GS detachment.

8

The along-coast coherence of PC1, and the robust 2-3 month lag between off-shelf and coastal sea level variability (see offshore region in Fig. 3), inform hypotheses about the underlying oceanic mechanisms controlling the propagation of sea level anomalies from the off-shelf region to the coast (e.g., Wu & He, 2025). Our results are consistent with propagation along the continental slope via topographic Rossby waves (e.g., Wise et al., 2018; Hughes et al., 2019; Wise et al., 2020). The latter travel with a speed of a few centimeters per second at these latitudes (first baroclinic mode), roughly consistent with the time lag we quantified between the off-shelf region and the PC1 (barotropic Rossby waves may also be involved in this transfer process). Once sea level anomalies break the potential vorticity barrier and penetrate onto the shallow continental shelf (e.g., Wise et al., 2020), they are transmitted via Kelvin waves traveling at a few meters per second (first baroclinic mode); such signals can travel from Cape Hatteras to the Gulf of Mexico in less than a month. This lag is not resolved using the monthly SSH fields available from the HR RYF and is thus consistent with our identification of a single signed coastal mode. Given the disparity between open-ocean and coastal wave speeds, daily SSH fields will be required to capture the along-coast propagation of sea level anomalies.

The frequency band in which the along-coast intrinsic mode and the off-shelf region exhibit high coherence suggests that SSH within the off-shelf region might be influenced by variations in the GS position excited by intrinsic oceanic variability (e.g., Quattrocchi et al., 2012; Gregorio et al., 2015). More specifically, frequencies smaller than 0.9 year^{-1} seem consistent with interannual GS path oscillations, which are known to control a significant fraction of the total SSH variance within the GS detachment region (e.g., Guo et al., 2023). Related to this point, it is important to mention that the GS is often misplaced in numerical models (Chassignet & Marshall, 2008). This GS separation bias produces excessive surface EKE north of Cape Hatteras in POP (Parallel Ocean Program, Smith et al., (2010)) HR FOSI (Chassignet et al., 2020) and, therefore, we can expect that it may also impact the magnitude of the along-coast mode detected in the HR RYF simulation.

CESM simulations show that intrinsic sea level variability is smaller (in a time-aggregated sense) than forced sea level variability; however, it is not negligible and, as noted, may have inherent predictability. Although the origin of atmospherically-forced and intrinsic sea level variations is different, our study reveals that the oceanic mechanisms involved in the communication of off-shelf anomalies to the coast (and from Cape Hatteras to the Gulf of Mexico) are similar to those regulating the transfer of some previously described forced sea-level signals (e.g., Calafat et al., 2018; Dangendorf et al., 2021; 2023; Steinberg et al., 2024). As such, our findings help understand the role of GS path variations (forced and intrinsic) on coastal sea level, and we suggest that sea level forecasting efforts will benefit from further studies of intrinsic variability along the SEUS coastline and elsewhere. This study provides a better understanding of (i) the physical processes governing offshore-shelf and shelf-to-shelf communication along the SEUS coastline, and (ii) the relationship between offshore GS variations and coastal sea level (e.g., Ezer, 1995; 2013; Wu & He, 2025). It may also help with the interpretation of observational datasets (e.g., Oelsmann et al., 2024).

Appendix A. CESM simulations

We employed an HR FOSI simulation with a spatial resolution of 0.1° (~10 km) to analyze monthly SSH fields from 1993 to 2018. The HR FOSI simulation represents the response of the ocean and sea ice to prescribed atmospheric forcing (e.g., wind, temperature). This simulation was performed using the global Community Earth System Model version 1.3 (CESM1.3) following the Ocean Model Intercomparison Project version 2 (OMIP2) experimental protocol (Griffies et al., 2016). The 1958-2018 forcing applied is (nearly) identical in each of four consecutive cycles (or ensemble members) and is obtained from JRA55 reanalysis. The JRA55 atmospheric fields have a spatial resolution of 55 km and a temporal resolution of 3 hours. The HR FOSI simulation was initialized from observed climatology (i.e., World Ocean Atlas) and spun up through consecutive cycles of 1958-2018 (61-year) forcing. Each cycle repeats the forcing of the previous simulation (e.g., simulation years 62-122 (cycle 2) repeats the forcing of simulation years 1-61 (cycle 1)). Since the cycles share the same forcing but have different initial conditions, inter-cycle differences can be largely attributed to intrinsic processes.

The limited number of HR FOSI cycles does not allow a clear separation of forced and intrinsic variability (although estimation of the forced and intrinsic variance might be possible using inter-cycle differences, see Little et al. (2024)). To cleanly quantify intrinsic variability, we use an HR RYF (repeat-year forcing) simulation. The HR RYF simulation was carried out by applying a single year of JRA55 boundary conditions from May 2003 to the end of April 2004. The May 2003-April 2004 year is characterized by low (non-anomalous) values for major climate modes. The May-April cycle is to avoid forcing discontinuities in mid-winter. By applying the same annual forcing in each year, interannual variability in sea level can be mainly attributed to oceanic intrinsic processes. Here, we analyzed the last 32 years of monthly outputs from a 70-year-long HR RYF simulation to examine the spatiotemporal properties of intrinsic sea level variability along the SEUS coastline, over the continental shelf, and adjacent deep waters. The HR RYF simulation was selected because of its unprecedently high resolution (0.1°), which allows us to examine the linkage between offshore and along-coast intrinsic sea level variability. Further details of the model setup can be found in Little et al. (2024).

Appendix B. Observational dataset and comparisons with model outputs

We utilized monthly mean TG observations with less than 12 missing months over the 1993-2018 period. TG observations were obtained from the Permanent Service for Mean Sea Level Revised Local Reference database on December 1, 2022 (Holgate et al., 2013). Missing data were infilled using linear interpolation after removing the seasonal cycle from the time series.

Sea level recorded by TGs is affected by numerous processes not accounted for in CESM simulations (e.g., inverted barometer effect, barystatic changes, global mean steric expansion/contraction, and vertical land motion). Thus, we removed from the TG record (i) the inverted barometer effect, using surface pressure fields from the ERA-5 atmospheric reanalysis, and (ii) the global mean sea level due to barystatic and steric processes, employing estimates obtained from altimetry

(MeaSUREs, 2021). Additionally, we linearly detrended the corrected TG time series to account for vertical land motion (after correction and detrending, we denote sea level as ζ').

To compare model output and sea level observed by TGs, we extracted the SSH in the closest model grid points to each TG using a ball tree algorithm (i.e. a ball tree algorithm is an efficient means of finding model grid points closest to a list of TG locations; more details can be found https://scikit-learn.org/stable/modules/neighbors.html). The modelled time series were detrended to remove model drift. To evaluate the model performance at larger spatial scales, we compared the spatial structure of ζ' variability from the HR FOSI simulation with a 1/6° gridded satellite altimeter product at monthly temporal resolution over the 1993-2018 period (MeaSUREs, 2022). Before comparing the two datasets, we removed the global mean sea level and linearly detrended the residual at each grid point from the altimeter product (note that the inverted barometer effect has already been removed from the altimeter gridded product).

Appendix C. Additional data processing

SSH time series were extracted from the HR RYF simulation along the SEUS coast at 170 pseudo-TGs (one pseudo-TG for each model grid cell along the coast). Then, we applied Empirical Orthogonal Function (EOF) analysis on the extracted SSH time series to identify the modes that explain the largest fraction of variability in the dataset. First, a matrix (O) was created by storing the time series extracted from the HR RYF simulation along each column. Then, we computed the covariance matrix ($C = O^T O$) and solved the corresponding eigenvalue problem:

$$C = V\lambda V^T \tag{C1}$$

where V and λ are the eigenvector and eigenvalue matrices. Each eigenvalue indicates the fraction of the variance explained by each eigenvector. By expressing matrix O in the space identified by the eigenvectors, we computed the principal components (PCs) associated with each mode.

We also utilized coherence analysis to characterize the relationship between along-coast and offshore intrinsic sea level variability. The spectrum was obtained by applying a Hanning window with overlapping (50% overlap) data segments. Each data segment has a length of 64 time steps (i.e., 64 months) and starts halfway through the previous segment (i.e., each data segment captures half of the data of the previous one). Coherence uncertainties were obtained using a standard approach (e.g., Gallet & Julien, 2011). This approach sets a threshold to assess whether a computed coherence exceeds what might be expected from random noise. The threshold is determined based on the significance level (i.e., 95% significance level) and the number of segments used to compute the coherence spectrum. The number of segments was evaluated as the time series length divided by the window length multiplied by 0.5.

Data availability

Sea level observations analyzed in this study are available from the Permanent Service for Mean Sea Level (Holgate et al., 2013; Permanent Service for Mean Sea Level, 2024) (for tide gauges) and from NASA (MEaSUREs, 2021) (for

255 satellite altimetry). Derived quantities from CESM simulations, and scripts required to generate figures, are archived at Little (2024).

Author contribution

CD and CML conceptualized the study and performed the analyses. CD wrote the original draft. SGY ran the numerical simulations. CML, RMP, and SGY edited the draft and acquired funding.

260 **Competing interests**

The authors declare that they have no conflict of interest.

References

Bessières, L., Leroux, S., Brankart, J-M., Molines, J.-M., Moine, M.-P., Bouttier, P.-A., Penduff, T., Terray, L., Barnier, B.,
Sérazin, G., (2017). Development of a probabilistic ocean modelling systembased on NEMO 3.5: application at eddying
resolution. Geosci Model Dev 10:1091-1106. https://doi.org/10.5194/gmd-10-1091-2017

Calafat, F. M., Wahl, T., Lindsten, F., Williams, J., & Frajka-Williams, E. (2018). Coherent modulation of the sea-level
annual cycle in the United States by Atlantic Rossby waves. Nature communications, 9(1), 2571

Camargo, C. M., Piecuch, C. G., & Raubenheimer, B. (2024). From Shelfbreak to Shoreline: Coastal sea level and local
ocean dynamics in the Northwest Atlantic. Geophysical Research Letters, 51(14), e2024GL109583

Chang, P., Zhang, S., Danabasoglu, G., Yeager, S. G., Fu, H., Wang, H., ... & Wu, L. (2020). An unprecedented set of high-
resolution earth system simulations for understanding multiscale interactions in climate variability and change. Journal of
Advances in Modeling Earth Systems, 12(12), e2020MS002298

Chassignet, E. P., Yeager, S. G., Fox-Kemper, B., Bozec, A., Castruccio, F., Danabasoglu, G., . . . Xu, X. (2020). Impact of
horizontal resolution on global ocean–sea ice model simulations based on the experimental protocols of the Ocean Model
Intercomparison Project phase 2 (OMIP-2). Geosci. Model Dev., 13(9), 4595–4637. Retrieved from
https://gmd.copernicus.org/articles/13/4595/2020/ (Publisher: Copernicus Publications) doi: 10.5194/gmd-13-4595-2020

Close, S., Penduff, T., Speich, S., & Molines, J.-M. (2020). A means of estimating the intrinsic and atmospherically-forced
contributions to sea surface height variability applied to altimetric observations. 184, 102314. Retrieved 2023-03-11, from
https://linkinghub.elsevier.com/retrieve/pii/S0079661120300537 doi: 10.1016/j.pocean.2020.102314

Dangendorf, S., Frederikse, T., Chafik, L., Klinck, J. M., Ezer, T., & Hamlington, B. D. (2021). Data-driven reconstruction
reveals large-scale ocean circulation control on coastal sea level. Nature Climate Change, 11(6), 514-520

Dangendorf, S., Hendricks, N., Sun, Q., Klinck, J., Ezer, T., Frederikse, T., ... & Törnqvist, T. E. (2023). Acceleration of US
Southeast and Gulf coast sea-level rise amplified by internal climate variability. Nature Communications, 14(1), 1935

Donatelli, C., Ponte, R. M., Penduff, T., et al. Effects of oceanic intrinsic processes on the mean seasonal cycle in sea
level. ESS Open Archive. June 30, 2025. doi: 10.22541/essoar.175130702.25669481/v1

Ezer, T., Mellor, G. L., and Greatbatch, R. J. (1995). On the interpentadal variability of the North Atlantic Ocean: Model simulated changes in transport, meridional heat flux and coastal sea level between 1955–1959 and 1970–1974. Journal of Geophysical Research: Oceans, 100(C6), 10559-10566

300   Ezer, T., Atkinson, L. P., Corlett, W. B., and Blanco, J. L. (2013). Gulf Stream's induced sea level rise and variability along the US mid-Atlantic coast. Journal of Geophysical Research: Oceans, 118(2), 685-697

Forget, G., & Ponte, R. M. (2015). The partition of regional sea level variability. Progress in Oceanography, 137, 173-195

Frederikse, T., Simon, K., Katsman, C. A., & Riva, R. (2017). The sea-level budget along the Northwest Atlantic coast: GIA, 305   mass changes, and large-scale ocean dynamics. Journal of Geophysical Research: Oceans, 122(7), 5486-5501

Gallet, C., & Julien, C. (2011). The significance threshold for coherence when using the Welch's periodogram method: Effect of overlapping segments. Biomedical Signal Processing and Control, 6(4), 405-409

310   Gerkema, T., & Duran-Matute, M. (2017). Interannual variability of mean sea level and its sensitivity to wind climate in an inter-tidal basin. Earth System Dynamics, 8(4), 1223-1235

Gopal, A. (2022). The Impact of Horizontal Resolution on Projected Sea-Level Rise Along US East Continental Shelf With the Community Earth System Model. Journal of Advances in Modeling Earth Systems, 14(5). Retrieved 2022-05-18, from https://onlinelibrary.wiley.com/doi/10.1029/ 2021MS002868 doi: 10.1029/2021MS002868

315   Grégorio, S., Penduff, T., Sérazin, G., Molines, J. M., Barnier, B., & Hirschi, J. (2015). Intrinsic variability of the Atlantic meridional overturning circulation at interannual-to-multidecadal time scales. Journal of Physical Oceanography, 45(7), 1929-1946

Griffies, S. M., Danabasoglu, G., Durack, P. J., Adcroft, A. J., Balaji, V., Böning, C. W., . . . Yeager, S. G. (2016). OMIP contribution to CMIP6: experimental and diagnostic protocol for the physical 320   component of the Ocean Model Intercomparison Project. Geoscientific Model Development, 9(9), 3231– 3296. Retrieved 2018-06-27, from http://www.geosci-model-dev.net/9/ 3231/2016/ doi: 10.5194/gmd-9-3231-2016

Guo, Y., Bishop, S., Bryan, F., & Bachman, S. (2023). Mesoscale variability linked to interannual displacement of Gulf Stream. Geophysical Research Letters, 50(7), e2022GL102549

325   Hallberg, R. (2013). Using a resolution function to regulate parameterizations of oceanic mesoscale eddy effects. Ocean Modelling, 72, 92-103

Holgate, S. J., Matthews, A., Woodworth, P. L., Rickards, L. J., Tamisiea, M. E., Bradshaw, E., . . . Pugh, J. (2013). New Data Systems and Products at the Permanent Service for Mean Sea Level. Journal of Coastal Research, 29 (3), 493–504.
330   doi:10.2112/JCOASTRES-D-12-00175.1

Hughes, C. W., Fukumori, I., Griffies, S. M., Huthnance, J. M., Minobe, S., Spence, P., . . . Wise, A. (2019). Sea Level and the Role of Coastal Trapped Waves in Mediating the Influence of the Open Ocean on the Coast. Surveys in Geophysics, 40 (6), 1467–1492. Retrieved 2020-02- 18, from http://link.springer.com/10.1007/s10712-019-09535-x doi: 10.1007/s10712-019-09535-x

335   Huthnance, J. M. (2004). Ocean-to-shelf signal transmission: A parameter study. Journal of Geophysical Research, 109(C12). Retrieved 2018-10- 20, from http://doi.wiley.com/10.1029/2004JC002358 doi: 10.1029/ 2004JC002358

Li, D., Chang, P., Yeager, S. G., Danabasoglu, G., Castruccio, F. S., Small, J., . . . Gopal, A. (2022). The Impact of Horizontal Resolution on Projected Sea-Level Rise Along US East Continental Shelf with the Community Earth System Model. Journal of Advances in Modeling Earth Systems, 14(5). Retrieved 2022-05-18, from
340   https://onlinelibrary.wiley.com/doi/10.1029/ 2021MS002868 doi: 10.1029/2021MS002868

Little, C. M., Hu, A., Hughes, C. W., McCarthy, G. D., Piecuch, C. G., Ponte, R. M., & Thomas, M. D. (2019). The Relationship Between U.S. East Coast Sea Level and the Atlantic Meridional Overturning Circulation: A Review. Journal of Geophysical Research: Oceans, 124 (9), 6435–6458. Retrieved 2020-08-14, from https://onlinelibrary.wiley.com/doi/abs/ 10.1029/2019JC015152 doi: 10.1029/2019JC015152

345   Little, C. M., Yeager, S. G., Ponte, R. M., Chang, P., and Kim, W. M. (2024). Influence of Ocean Model Horizontal Resolution on the Representation of Global Annual-To-Multidecadal Coastal Sea Level Variability, J Geophys Res Oceans, 129, e2024JC021679, https://doi.org/https://doi.org/10.1029/2024JC021679

350   Long, X., Widlansky, M. J., Spillman, C. M., Kumar, A., Balmaseda, M., Thompson, P. R., et al. (2021). Seasonal forecasting skill of sea-level anomalies in a multi-model prediction framework. Journal of Geophysical Research: Oceans, 126, e2020JC017060. https:// doi.org/10.1029/2020JC017060

MEaSUREs. (2021). Global Mean Sea Level Trend from Integrated Multi-Mission Ocean Altimeters TOPEX/Poseidon, Jason-1, OSTM/Jason-2, and Jason-3 Version 5.1. NASA Physical Oceanography DAAC. Retrieved from
355   https://podaac.jpl.nasa.gov/dataset/MERGED TP J1 OSTM OST GMSL ASCII V51 doi: 10.5067/GMSLM-TJ151

MEaSUREs. (2022). MEaSUREs Gridded Sea Surface Height Anomalies Version 2205. NASA Physical Oceanography DAAC. Retrieved from https://podaac.jpl.nasa.gov/dataset/SEA SURFACE HEIGHT ALT GRIDS L4 2SATS 5DAY 6THDEG V JPL2205 doi: 10.5067/SLREF-CDRV3

NOAA. (2022). A NOAA capability for Coastal Flooding and Inundation Information and Services at Climate Timescales to
360   Reduce Risk and Improve Resilience. Retrieved from https://cpo.noaa.gov/Portals/0/ Docs/Risk-Teams/NOAA-Coastal-Inundation-at-Climate-Timescales -Whitepaper.pdf

Oelsmann, J., Calafat, F. M., Passaro, M., Hughes, C., Richter, K., Piecuch, C., ... & Jevrejeva, S. (2024). Coherent modes of global coastal sea level variability. Journal of Geophysical Research: Oceans, 129(12), e2024JC021120

Penduff, T., Juza, M., Brodeau, L., Smith, G. C., Barnier, B., Molines, J.-M., . . . Madec, G. (2010). Impact of global ocean
365   model resolution on sea-level variability with emphasis on interannual time scales. Ocean Sci., 6(1), 269–284. Retrieved 2014-05-23, from http://www.ocean-sci.net/6/269/ 2010/ (bibtex: penduff2010) doi: 10.5194/os-6-269-2010

Penduff, T., Juza, M., Barnier, B., Zika, J., Dewar, W. K., Treguier, A.-M., . . . Audiffren, N. (2011). Sea Level Expression of Intrinsic and Forced Ocean Variabilities at Interannual Time Scales. Journal of Climate, 24(21), 5652–5670. Retrieved 2023-03-11, from http://journals.ametsoc.org/doi/ 10.1175/JCLI-D-11-00077.1 doi: 10.1175/JCLI-D-11-00077.1

370   Penduff, T., Barnier, B., Terray, L., Bessières, L., Sérazin, G., Gregorio, S., ... & Brasseur, P. (2014). Ensembles of eddying ocean simulations for climate. CLIVAR Exchanges, Special Issue on High Resolution Ocean Climate Modelling, 19

Penduff, T., Llovel, W., Close, S. et al. (2019). Trends of Coastal Sea Level Between 1993 and 2015: Imprints of Atmospheric Forcing and Oceanic Chaos. Surv Geophys 40, 1543–1562. https://doi.org/10.1007/s10712-019-09571-7
375   Permanent Service for Mean Sea Level (PSMSL), 2024, "Tide Gauge Data", Retrieved 09 Sep 2024 from http://www.psmsl.org/data/obtaining/

Piecuch, C. G., Bittermann, K., Kemp, A. C., Ponte, R. M., Little, C. M., Engelhart, S. E., & Lentz, S. J. (2018). River-discharge effects on United States Atlantic and Gulf coast sea-level changes. Proceedings of the National Academy of
380   Sciences, 115(30), 7729-7734

Quattrocchi, G., Pierini, S., and Dijkstra, H. A. (2012). Intrinsic low-frequency variability of the Gulf Stream, Nonlin. Processes Geophys., 19, 155–164, https://doi.org/10.5194/npg-19-155-2012

385 Qiu, B., Chen, S., Wu, L., and Kida, S. (2015). Wind-versus eddy-forced regional sea level trends and variability in the North Pacific Ocean. Journal of Climate, 28(4), 1561-1577

Rashid, M. M., Wahl, T., & Chambers, D. P. (2021). Extreme sea level variability dominates coastal flood risk changes at decadal time scales. *Environmental Research Letters*, *16*(2), 024026

390 Sérazin, G., Penduff, T., Gregorio, S., Barnier, B., Molines, J.-M., & Terray, L. (2015). Intrinsic Variability of Sea Level from Global Ocean Simulations: Spatiotemporal Scales. Journal of Climate, 28(10), 4279–4292. Retrieved 2018-06-27, from http://journals.ametsoc.org/doi/10.1175/ JCLI-D-14-00554.1 doi: 10.1175/JCLI-D-14-00554.1

Sérazin, G., Penduff, T., Barnier, B., Molines, J. M., Arbic, B. K., Müller, M., & Terray, L. (2018). Inverse cascades of kinetic energy as a source of intrinsic variability: A global OGCM study. Journal of Physical Oceanography, 48(6), 1385-
395 1408

Smith, R., Jones, P., Briegleb, B., Bryan, F., Danabasoglu, G., Dennis, J., Dukowicz, J., Eden, C., Fox-Kemper, B., Gent, P., Hecht, M., Jayne, S., Jochum, K. L. M., Large, W., Maltrud, M., Nor- ton, N., Peacock, S., Vertenstein, M., and Yeager, S. (2010). The parallel ocean program (POP) reference manual: ocean component of the community climate system model (CCSM) and community earth system model (CESM), Rep. LAUR-01853, 141, 1–140

400 Steinberg, J. M., Griffies, S. M., Krasting, J. P., Piecuch, C. G., & Ross, A. C. (2024). A Link between US East coast sea level and North Atlantic subtropical ocean heat content. Journal of Geophysical Research: Oceans, 129(12), e2024JC021425

Thatcher, C. A., Brock, J. C., & Pendleton, E. A. (2013). Economic vulnerability to sea-level rise along the northern US Gulf Coast. *Journal of Coastal Research*, (63), 234-243

Vinogradov, S. V., & Ponte, R. M. (2011). Low-frequency variability in coastal sea level from tide gauges and altimetry.
405 Journal of Geophysical Research, 116(C7). Retrieved 2018-06-27, from http://doi.wiley.com/10.1029/ 2011JC007034 doi: 10.1029/2011JC007034

Wang, O., Lee, T., Frederikse, T., Ponte, R. M., Fenty, I., Fukumori, I., & Hamlington, B. D. (2024). What forcing mechanisms affect the interannual sea level co-variability between the northeast and southeast coasts of the United States?. Journal of Geophysical Research: Oceans, 129(1), e2023JC019873

410   Wise, A., Hughes, C. W., & Polton, J. A. (2018). Bathymetric Influence on the Coastal Sea Level Response to Ocean Gyres at Western Boundaries. Journal of Physical Oceanography, 48 (12), 2949–2964. Retrieved 2019-03-07 from http://journals.ametsoc.org/doi/10.1175/JPO-D-18-0007.1 doi: 10.1175/JPO-D-18-0007.1

Wise, A., Polton, J. A., Hughes, C. W., & Huthnance, J. M. (2020). Idealised modelling of offshore-forced sea level hot spots and boundary waves along the North American East Coast. Ocean Modelling, 155, 101706. Retrieved 2020-10-19,
415   from https://linkinghub.elsevier.com/retrieve/pii/S1463500320302080 doi: 10.1016/j.ocemod.2020.101706

Wu, T., & He, R. (2025). Gulf Stream near Cape Hatteras modulates sea level variability along the southeastern coast of North America. Geophysical Research Letters, 52, e2024GL112776. https://doi.org/10.1029/2024GL112776

Yeager, S. G., Chang, P., Danabasoglu, G., Rosenbloom, N., Zhang, Q., Castruccio, F. S., ... and Simpson, I. R. (2023). Reduced Southern Ocean warming enhances global skill and signal-to-noise in an eddy-resolving decadal prediction
420   system. npj Climate and Atmospheric Science, 6(1), 107